9th ANKARA INTERNATIONAL AEROSPACE CONFERENCE AIAC-2017-064
20-22 September 2017 - METU, Ankara TURKEY

OPTIMIZATION OF COMPLIANT PARTS OF A TRAILING EDGE CONTROL SURFACE OF A MORPHING WING

Pınar Arslan[1]
Middle East Technical University
Ankara, Turkey

Ercan Gürses[2]
Middle East Technical University
Ankara, Turkey

ABSTRACT

In this study, optimization analyses are conducted for compliant parts of a hybrid trailing edge control surface of an unmanned aerial vehicle. The geometry of the control surface was taken from a previous study [Tunçöz, 2015] and regenerated parametrically. Its finite element model is created by using ANSYS software. Then, the optimization analyses are conducted by ANSYS v15.0 Workbench Design Exploration module. The input parameters of the optimization are the dimensions and materials of the compliant parts and the actuation amounts of the servos. The aim of the optimization study is to achieve the required tip deflection of the control surface with minimum servo torque.

INTRODUCTION

Morphing aircraft is defined as “Multi-role aircraft that change their external shape substantially to adapt to a changing mission environment during flight” [Barbarino, 2011]. Compared to conventional aircraft, morphing aircraft have certain advantages. They can be optimized for several flight phases in terms of aerodynamic performance while conventional aircraft are mainly optimized for a single flight phase. Moreover, flight envelope of the conventional aircraft can be extended due to its flexibility against different conditions. Recent developments of new materials and design techniques have led to morphing concept being more applicable and attractive in the aviation field [Smith, 1990]. For this reason, in this study different compliant materials and geometries are examined for the optimization of the flexible skin parts in a hybrid trailing edge control surface.

This study has been conducted under the scope of CHANGE (**C**ombined morp**H**ing **A**ssessment software usi**NG** flight **E**nvelope data and mission based morphing prototype wing development) Project. It is a collaborative project of the 7th framework program of the European commission with 9 partners, one of which is METU. The aim of this project is association of four different morphing mechanisms to one unmanned air vehicle (UAV) [CHANGE Project, 2012]. Baseline wing of the UAV shown in Figure 1 has the NACA 6510 profile with no twist in span direction. Within the scope of the project, a hybrid trailing edge control surface which consists of different parts, namely C, compliant and rigid parts, was

[1] Pınar Arslan, Email: pinar.arslan@tai.com.tr
[2] Assoc. Prof. Dr. in a Aerospace Engineering Department, Email: gurses@metu.edu.tr

designed by METU [Tunçöz, 2015]. Figure 3 shows the control surface and its parts. The aim of this study is optimization of the compliant parts of the control surface for all missions by changing the skin material and dimensions of the compliant part and the amounts of actuations of servo actuators.

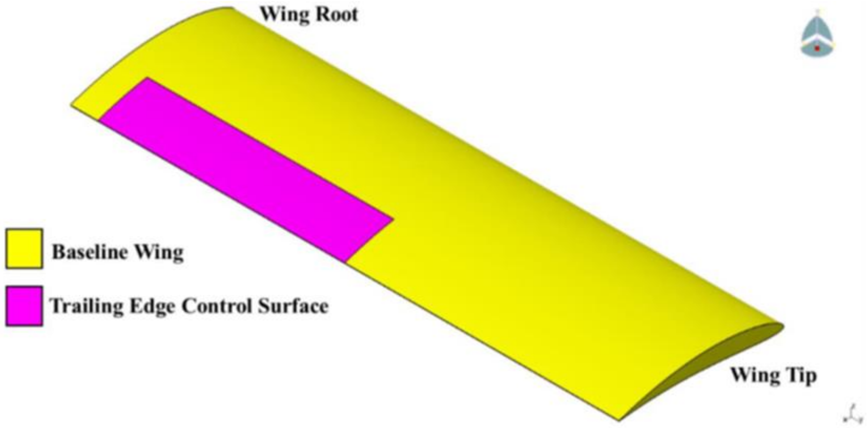

Figure 1: Baseline wing of the UAV [Tunçöz, 2015]

The mission profile of the morphing UAV and corresponding NACA profiles are shown in Figure 2 [CHANGE Project, 2012]. The main aim is to provide the transition between these NACA profiles while designing the trailing edge control surface which is explained in the next part.

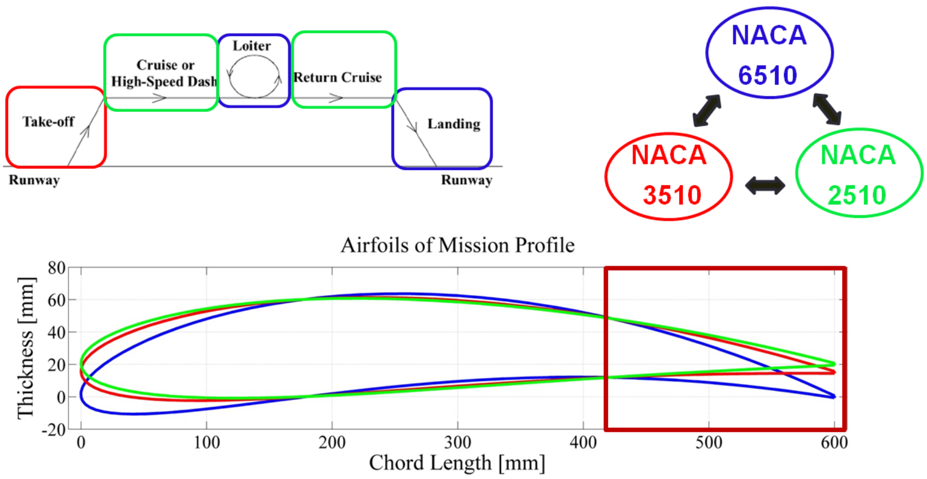

Figure 2: The mission profile of the UAV and corresponding NACA profiles

Design of the Hybrid Trailing Edge Control Surface

Two different hybrid control surface designs shown in Figure 3, which are open cell and closed cell designs, were generated in CATIA V5 R-6R2012 package software in a previous study [Tunçöz, 2015]. Both designs consist of a C part, a compliant part and a rigid part. The C part is used for the connection of the control surface to the wing and made of a stiff material. It is assumed as rigidly connected to the wing. The compliant part is made of a flexible material, so it can undergo significant amount of deformation and therefore the control surface can deflect. Upper and lower compliant parts stretch by different amounts by the servo actuators. The difference between these two designs is that there is a gap between the transmission part of the open cell control surface design. The dimensions and materials of these parts are presented in Table 1. The C part and the rigid part properties for both designs are kept as in Table 1. Since the main focus of this study is the compliant part, the thickness and material of this part are initially taken as in Table 1 and changed iteratively during the optimization analyses.

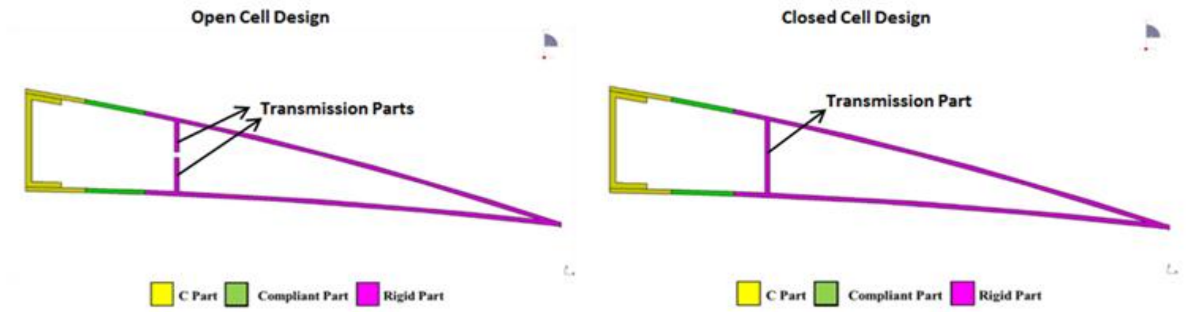

Figure 3: Open Cell and Closed Cell Control Surface Designs and their parts

Table 1: Thickness and materials of the parts of the control surface designs

	C Part		Compliant Part	Rigid Part
	Bar part	Skin parts		
Material	Aluminum	Aluminum	Neoprene Rubber	Aluminum
Thickness [mm]	2.0	1.5	1.5	1.5

In the control surface design, four identical servo actuators are used for the actuation of upper (two blue servo actuator) and lower parts (two red servo actuators) of the control surface. Due to the tight geometry of the control surface, the servo actuator, Volz DA 13-05-60, which has the smallest dimension and maximum available torque was chosen [Tunçöz, 2015]. Figure 4 shows the placements of the servo actuators in the control surface. Moreover, the details of the servo actuator and the designed fastener for the connection to C part are shown in Figure 4 [Volz Servos; Tunçöz, 2015].

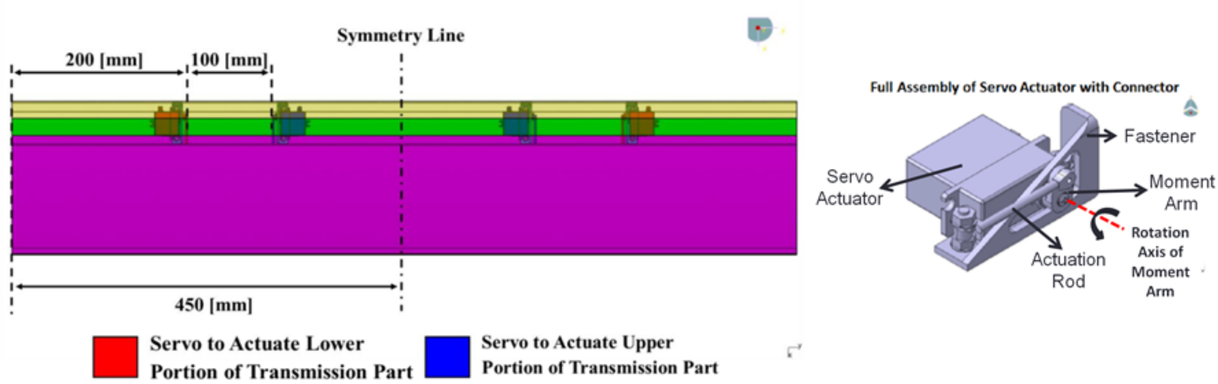

Figure 4: Locations of the servo actuators on the control surface and full assembly of the servo actuators

Finite Element Model of the Trailing Edge Control Surface

The finite element model of the control surface designs presented in Figure 5 are created by using Static Structural module of ANSYS v15.0 Workbench according to the mesh convergence study conducted in a previous study [Arslan, 2014]. Since the C part of the control surface is rigidly connected to the wing and is made of a stiff material, its effect on the analyses is assumed to be negligible. Therefore, it is not taken into account in the finite element models for the two designs.

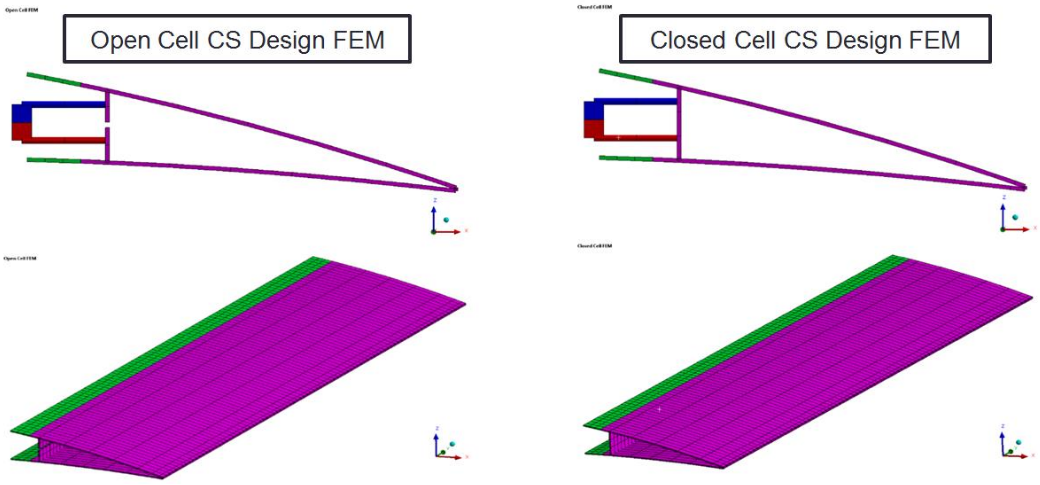

Figure 5: Finite Element Models of the control surface designs

As mentioned in the previous part, the control surface consists of different pieces, named as rigid part, compliant parts and transmission parts. In this study, it is assumed that these pieces are perfectly connected to each other. Moreover, the control surface is fixed at the edges of compliant parts with 'Fixed Support' option of ANSYS. In order to model the weight of the control surface 'Standard Earth Gravity' is applied to the finite element model. Moreover, coinciding nodes of moment arms and actuation rods are coupled except rotation about span-wise direction to model the pinned joint. The coinciding nodes are depicted as green in Figure 6. Also, the connection between the actuation rods of the servo actuators and transmission parts are modeled with 'Bonded Contact' option of ANSYS. All the boundary conditions and contacts of finite element model are presented in Figure 6. In this study, due to large deflections and material nonlinearities, nonlinear finite element analyses are conducted.

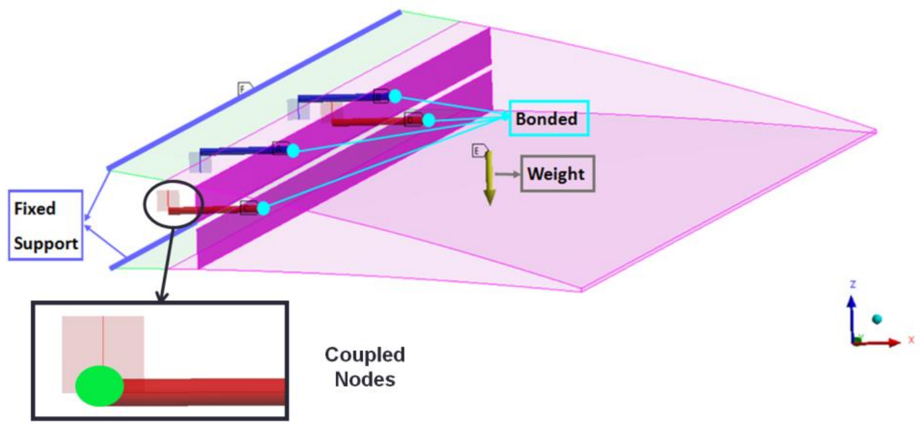

Figure 6: Boundary Conditions and Contacts of the Finite Element Model

METHOD

After generation of the finite element models of the control surface designs, the method, inputs, objectives, constraints and targets of the optimization analyses are identified. For the optimization analyses in this study, Design Exploration tool of ANSYS is used. Three different optimization methods, which are Screening, Multi-Objective Genetic Algorithm (MOGA) and Adaptive Multiple-Objective Genetic Algorithm (AMO), are available in Design

Exploration tool for multi-objective problems. Screening method is a non-iterative approach and it generally used for preliminary designs. The second one, MOGA is an iterative method and it is more refined than Screening. The third one, AMO, uses the same general approach with MOGA. However, it evaluates the results with Kriging error predictor and it reduces the necessary time to obtain an optimum point [ANSYS Design Exploration Users Guide, 2015]. Therefore, AMO method is selected for the optimization analyses in this study.

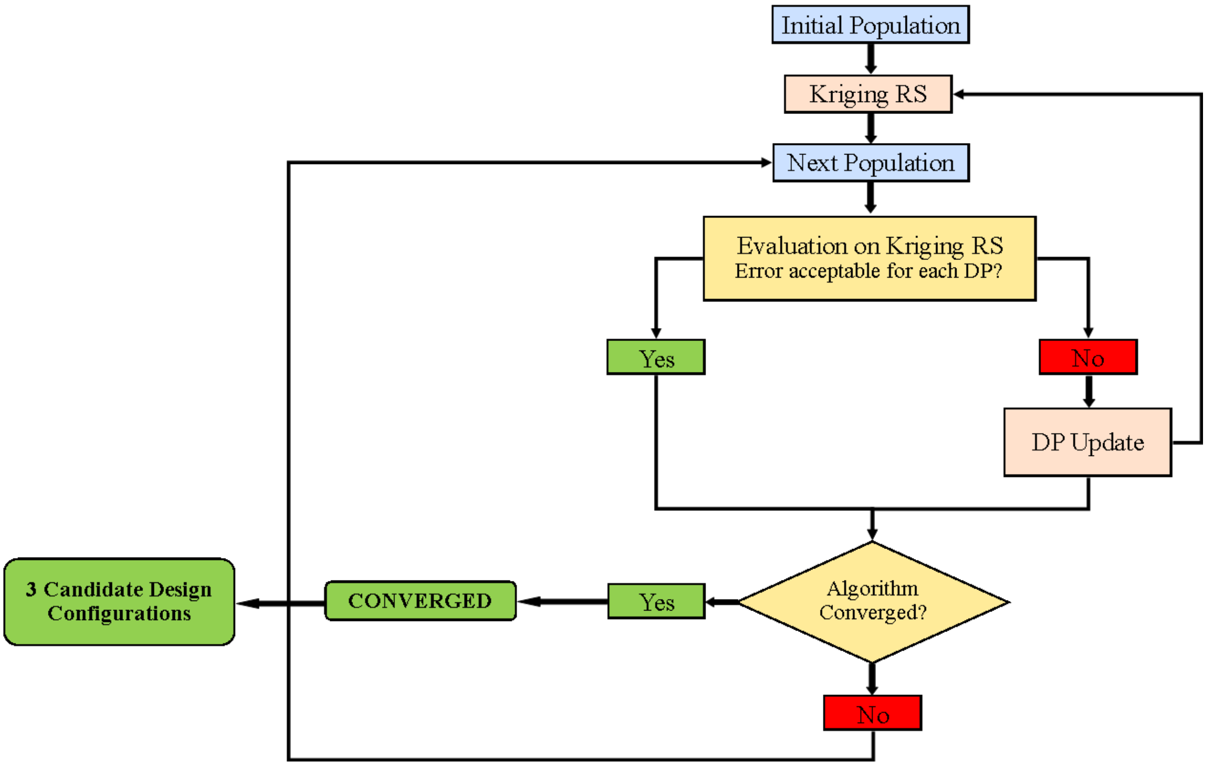

Figure 7: Workflow schema of the Adaptive Multiple-Objective Optimization Method

The workflow of AMO method is shown in Figure 7. It is explained step by step as follows [ANSYS Design Exploration Users Guide, 2015]:

1. Initial population is created in order to construct the Kriging response surface.
2. Then, the Kriging response surface is obtained by conducting finite element analyses of this initial population.
3. By using MOGA algorithm, next population is created.
4. Then, these points are evaluated by using the Kriging response surface.
    a. If the errors for the points are acceptable, algorithm convergence of these points are checked.
    b. If the errors for the design points are not acceptable, these points are updated by finite element analyses and sent to Kriging response surface step to improve the response surface. Also, the updated design points are sent to convergence check step.
5. Convergence check for the population is performed.
    a. If the algorithm is not converged, new population is generated.
    b. If it is converged, then optimization is finished.

In multi objective algorithms generally the output is not a single result. For this reason number of outputs, which are candidate points, are decided as 3 in this work.

Optimization Inputs

In this study, during optimization analyses, which are performed in vacuo condition, three main factors are changed iteratively. First of them is the material used for the compliant parts. The motion of the control surface is achieved by axial stretching of the upper and lower compliant parts. For this reason, the most important property of the material is axial deformation behavior. Hyperelastic materials have the ability of undergoing large deformations under small loads. Moreover, they can retain their original shape after applied loads are removed. To this end, four different hyperelastic materials, which are Neoprene Rubber, Sample Elastomer-1 (SE-1), Sample Elastomer-2 (SE-2) and Silicone, are used in the compliant parts. Neoprene Rubber, Sample Elastomer-1 and Sample Elastomer-2 are taken from the ANSYS material library [ANSYS, 2015]. The fourth material, Silicone, is provided by a project partner INVENT Company [INVENT, 2016]. The stress-strain curve of this material is obtained by a uniaxial tensile test conducted in METU Department of Aerospace Engineering. The stress-strain curves of the hyperelastic materials are provided to ANSYS software for the analyses. Having these stress-strain data, a proper curve fitting is applied to stress-strain data. Then, suitable curve fits are obtained for each material by using ANSYS software. Figure 8 shows the uniaxial test data of the hyperelastic materials and the corresponding curve fits.

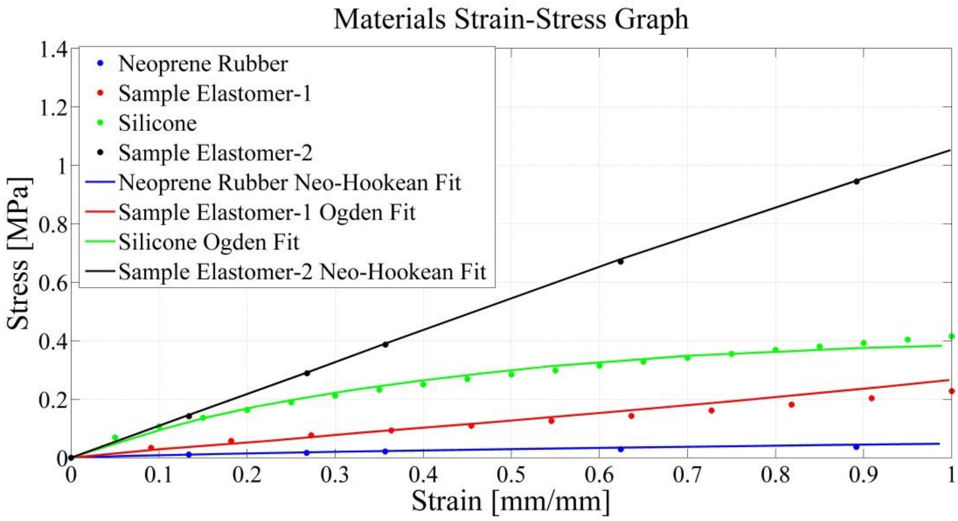

Figure 8: Uniaxial test data of the hyperelastic materials and the corresponding curve fits

Second optimization variable is the dimensions of the compliant parts. The variable dimensions are the thicknesses and lengths of the compliant parts as shown in Figure 9. These dimensions are modeled parametrically by using Design Modeler tool of ANSYS Workbench.

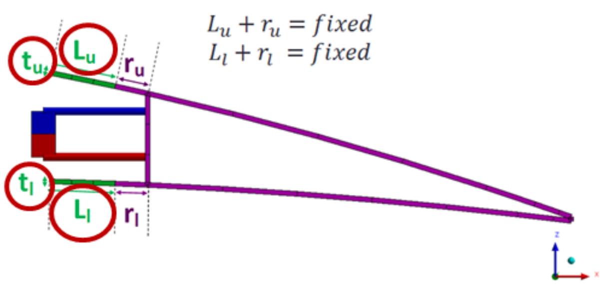

Figure 9: Variable dimensions of the upper and lower compliant parts of the control surface

The last optimization variable is the amounts of actuations of the servo actuators. Note that, the servo actuators are not completely modeled in the finite element model. Only actuation rods and moment arms shown in Figure 10 are modeled as aluminum beams [ANSYS, 2015]. Rotations are applied to the moment arms in the direction of red and blue arrows shown in Figure 10 and consequently the motion of the control surface is generated.

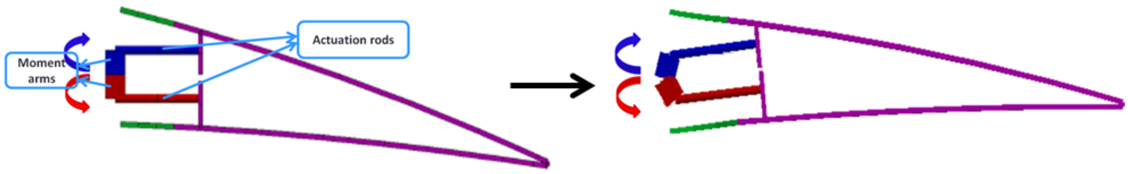

Figure 10: Moment arms and actuation rods of the servo actuators and the motion of the control surface

Optimization Target, Objectives and Constraints

After optimization method and inputs are determined, optimization target, objectives and constraints are identified.

The target of the optimization is the tip deflection of the control surface. In order to achieve to morph the control surface to the NACA 2510 profile, the upward tip deflection of 20.2 mm is needed.

The objectives of the optimization problem are to minimize the torque reactions of the servo actuators.

The first constraint is that the maximum torque reactions are limited with the limits of the selected servo actuators. The second one is the chord-wise normal strains in compliant parts. These strain values must be positive because, any compression in the compliant parts yields slacking and it is not desired. Also, it is decided that the maximum normal strains must be less than 1. Lastly, the maximum and the minimum combined stresses of the moment arms and actuation rods are limited to yield stress of aluminum. The optimization target, objectives and constrains are listed in Table 2.

Using the explained target, objectives and constraints, in total eight discrete optimization studies are conducted with four different materials and for two different designs.

RESULTS AND CONCLUSION

After all the analyses are conducted, it is seen that the optimization analyses have converged only for two materials which are the Neoprene Rubber and the Sample Elastomer-1. The control surfaces with compliant parts made of Sample Elastomer-2 and Silicone, could not achieve the desired tip deflection with the available torque of the servo actuators. Output of each converged analysis is three best candidate design points depicted as CP which are shown in Table 3. The abbreviations of the name of the output parameters are given in Table 2.

Table 2: Output parameters and their abbreviations

Output Parameters	Explanation
d_z	Tip deflection in z-direction
Q_l	Torque reaction of the servo to actuate the lower part
Q_u	Torque reaction of the servo to actuate the upper part
$\sigma_{c_{min}}$	Minimum combined stress of the beams
$\sigma_{c_{max}}$	Maximum combined stress of the beams
$\epsilon_{u_{min}}$	Minimum normal elastic strain of the upper compliant part
$\epsilon_{l_{min}}$	Minimum normal elastic strain of the lower compliant part
$\epsilon_{u_{max}}$	Maximum normal elastic strain of the upper compliant part
$\epsilon_{l_{max}}$	Maximum normal elastic strain of the lower compliant part

Table 3: Results of 3 candidate design points for each materials of the compliant parts of the control surface

	Material	CPs	d_z [mm]	Q_l [Nmm]	Q_u [Nmm]	$\sigma_{c_{min}}$ [MPa]	$\sigma_{c_{max}}$ [MPa]	$\epsilon_{u_{min}}$ [-]	$\epsilon_{l_{min}}$ [-]	$\epsilon_{u_{max}}$ [-]	$\epsilon_{l_{max}}$ [-]
Open Cell	Neoprene Rubber	**CP1**	20.47	491.31	165.54	-52.05	36.07	0.19	0.17	0.26	0.22
		CP2	19.93	501.78	172.47	-54.88	38.48	0.20	0.17	0.26	0.23
		CP3	19.97	526.65	226.58	-43.36	26.34	0.16	0.14	0.23	0.20
	SE-1	CP4	20.42	743.39	169.69	-23.38	19.28	0.12	0.15	0.19	0.20
		CP5	20.53	760.28	83.19	-23.81	19.82	0.10	0.15	0.17	0.21
		CP6	20.47	760.36	74.79	-23.81	19.82	0.10	0.15	0.17	0.21
Closed Cell	Neoprene Rubber	CP7	20.2	555.63	104.96	-241.07	224.97	0.16	0.15	0.29	0.20
		CP8	20.2	587.31	117.99	-242.63	225.47	0.16	0.19	0.29	0.23
		CP9	18.37	518.64	52.26	-224.90	209.93	0.19	0.14	0.31	0.19
	SE-1	CP10	19.77	856.09	64.78	-205.79	179.52	0.07	0.16	0.17	0.21
		CP11	20.34	876.36	26.57	-198.24	171.57	0.05	0.14	0.17	0.19
		CP12	20.10	1165.97	208.58	-218.30	181.93	0.04	0.17	0.12	0.23

According to Table 3, all the candidate points achieve nearly the target of the optimization analyses, which is 20.2 mm the tip deflection of the control surface. Moreover, all the minimum strain values of the compliant parts of the control surface are positive. In other words, there is no compression in the compliant parts as desired. Also, the maximum strains of the lower and upper compliant parts are under one hundred percent, which is the maximum strain limit in the optimization study. However, one optimum point must be selected among the results in Table 3. Therefore, the optimum design is chosen by looking at the combined stresses and servo torque requirements. Table 3 indicates that open cell design is clearly much more preferable due to the lower combined stress values of the moment arms and actuation rods in comparison to the closed cell design. Moreover, it is seen that, all the torque reactions of the servos which actuate the upper part are smaller than the torque reactions of the servos which actuate the lower part of the control surface. The candidate, which has the least torque values among the others of lower part, is seen as the first one, CP1. Thus, the optimum design is selected as open cell control surface design with Neoprene Rubber compliant parts. Table 4 demonstrates the inputs of three best design points for each material in the optimization analyses. Then, the inputs of the optimum design point, CP1, are simplified simply by rounding numbers considering manufacturability of the control surface.

Table 4: Three best candidate points of the optimization analyses

Design	Material	CPs	Lower Servo Rotation [deg]	Upper Servo Rotation [deg]	Lower Compliant Thickness [mm]	Upper Compliant Thickness [mm]	Lower Compliant Length [mm]	Upper Compliant Length [mm]
Open Cell	Neoprene Rubber	**CP1**	-35.60	18.91	1.00	1.92	21.36	3.10
		CP2	-36.04	19.62	1.04	1.87	20.80	3.48
		CP3	-33.93	17.56	1.21	1.89	24.20	3.18
	SE-1	CP4	-34.91	18.66	1.16	1.58	23.79	4.10
		CP5	-33.70	17.32	1.07	1.58	22.51	3.76
		CP6	-33.69	17.33	1.06	1.56	22.39	3.80
Closed Cell	Neoprene Rubber	CP7	-34.16	19.67	1.23	1.94	24.12	3.04
		CP8	-34.18	19.67	1.23	1.93	19.98	3.03
		CP9	-32.78	19.61	1.23	1.93	24.02	3.04
	SE-1	CP10	-32.93	18.81	1.07	1.64	21.78	5.50
		CP11	-31.26	16.65	1.13	1.60	23.78	3.92
		CP12	-32.86	18.27	1.34	1.89	20.42	7.66

The rounded inputs of the optimum design CP1 are shown in Table 5 and the corresponding results to these inputs obtained by a finite element analysis are presented in Table 6. The deflection of the control surface in z direction during morphing from NACA 6510 to NACA 2510 profile is shown in Figure 11.

Table 5: The simplified optimum design configuration of control surface

Design	Lower Servo Rotation [deg]	Upper Servo Rotation [deg]	Lower Compliant Thickness [mm]	Upper Compliant Thickness [mm]	Lower Compliant Length [mm]	Upper Compliant Length [mm]
Simplified Design	-35.50	19.00	1.00	1.90	21.00	3.00

Table 6: Corresponding results of the finite element analysis of the simplified optimum design given in Table 5

Design	d_z [mm]	Q_l [Nmm]	Q_u [Nmm]	$\sigma_{c_{min}}$ [MPa]	$\sigma_{c_{max}}$ [MPa]	$\epsilon_{u_{min}}$ [-]	$\epsilon_{l_{min}}$ [-]
Simplified Design	20.26	485.15	150.17	-52.00	36.24	0.20	0.17

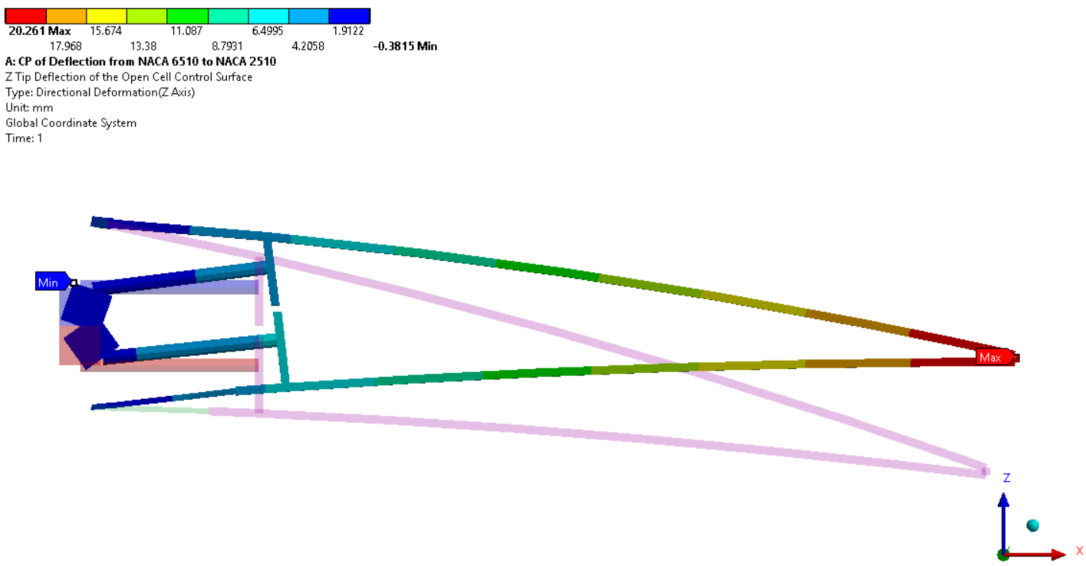

Figure 11: Deflection of the simplified control surface design in z direction in case of morphing from NACA 6510 to NACA 2510 profile

In conclusion, the selected control surface could do each maneuver in its' mission profile with a most efficient way in terms of torque requirements, the combined beam stresses and the strain values of the compliant parts. Furthermore, according to the optimum design inputs and outputs, Neoprene Rubber is the most flexible and appropriate material among the considered materials to be use in the compliant skin for this design. The combined beam stress results are found to be much lower for the open cell design. The open cell is more flexible than the closed cell design due to its gap in the transmission part. Thus, the open cell design is more favorable. Moreover, the torque requirements of the servo actuators decrease, when the lower compliant skin is thinner and the upper compliant skin is thicker. The torque requirements also decrease when the upper compliant part is shorter and the lower compliant part is longer.

Acknowledgement

The work presented herein has been partially funded by the European Community's Seventh Framework Program (FP7) under the Grant Agreement 314139. The CHANGE project ("Combined morphing assessment software using flight envelope data and mission based morphing prototype wing development") is a L1 project funded under the topic AAT.2012.1.1-2 involving nine partners. The project started in 1 August, 2012.

The study is supported by Turkish Aerospace Industries, Inc.

References

ANSYS Design Exploration Users Guide, Canonsburg, PA, (2015)

ANSYS Inc, *Workbench Material Library,* Canonsburg, PA, (2015)

Arslan, P., Kalkan, U., Tıraş, H., Tunçöz, İ.O., Yang, Y., Gürses, E., Şahin, M., Özgen, S., and Yaman, Y. (2014) *Structural Analysis of an Unconventional Hybrid Control Surface of a Morphing Wing,* ICAST2014: 25th International Conference on Adaptive Structures and Technologies, p:6-8, Oct 2014.

Barbarino, S., Bilgen, O., Ajaj, R. M., Friswell, M. I., and Inman, D. J. (2011) *A review of morphing aircraft*, Journal of Intelligent Material Systems and Structures, Vol. 22, No. 9, p: 823–877.

CHANGE Project, *"CHANGE Project Summary,"* http://change.tekever.com/partnership, 2012, [Online; accessed 16-November-2016].

INVENT GmbH, http://www.invent-gmbh.de/, [Online; accessed 16-November-2016].

Smith, S. B. and Nelson, D. W. (1990) *Determination of the aerodynamic characteristics of the mission adaptive wing,* Journal of Aircraft, Vol. 27, No. 11, p 950-958.

Tunçöz, İ.O. (2015) *Design and Analysis of a Hybrid Trailing Edge Control Surface of a Fully Morphing Unmanned Aerial Vehicle Wing,* Master's thesis, Middle East Technical University, February 2015

Volz Servos, http://www.volz-servos.com/English/13mmClass/, [Online; accessed 05-December-2014].